applied sciences

MDPI

Article

Effects of Loading Modes on Fatigue Limit Estimation in Terms of Rotating Bending Fatigue and Rate Process Theory

Mai Fukami [1,*], Noriyasu Oguma [2], Benjamin Guennec [3], Noriyo Horikawa [3] and Tatsuo Sakai [4]

1 Graduate School of Science and Engineering, University of Toyama, Gofuku 3190, Toyama 930-8555, Japan
2 Faculty of Engineering, University of Toyama, Gofuku 3190, Toyama 930-8555, Japan; oguma@eng.u-toyama.ac.jp
3 Department of Mechanical Systems Engineering, Toyama Prefectural University, Kurokawa 5180, Imizu, Toyama 939-0398, Japan; bguennec@pu-toyama.ac.jp (B.G.); horikawa@pu-toyama.ac.jp (N.H.)
4 Research Organization of Science and Technology, Ritsumeikan University, Kusatsu Shiga 525-8577, Japan; sakai@se.ritsumei.ac.jp
* Correspondence: m.fukami@tohshin-inc.co.jp

Abstract: In this study, the influence of loading modes on the fatigue limit estimation of low-to-medium-carbon steels was modeled in terms of the rate process theory proposed by Guennec et al. The axial loading model established in terms of the rate process theory has been shown to be effective for axial loading fatigue, but its applicability to rotating bending fatigue is uncertain. Therefore, low- and medium-carbon steels were tested for rotating bending fatigue, and the fatigue limits obtained were compared with those estimated by the axial loading model established in terms of the rate process theory. However, since the model could not be applied, we propose a new model in which the material parameters of an estimation equation established in terms of the rate process theory are expressed based on Vickers hardness, which was introduced to improve the usability of the model. It was found that there was a discrepancy between the axial load fatigue limit and the rotating bending fatigue limit due to the effect of the loading mode. To solve this discrepancy, the stress index was introduced into the model. The proposed model provides a method for estimating the frequency-dependent fatigue limits for different loading modes.

Keywords: fatigue limit estimation; rotating bending fatigue; Vickers hardness; *S-N* curves; rate process theory

Citation: Fukami, M.; Oguma, N.; Guennec, B.; Horikawa, N.; Sakai, T. Effects of Loading Modes on Fatigue Limit Estimation in Terms of Rotating Bending Fatigue and Rate Process Theory. *Appl. Sci.* **2024**, *14*, 477. https://doi.org/10.3390/app14020477

Academic Editor: Guian Qian

Received: 21 November 2023
Revised: 24 December 2023
Accepted: 3 January 2024
Published: 5 January 2024

1. Introduction

To realize the fatigue limit design of mechanical structures, it is necessary to clearly understand the fatigue limit of materials through conducting fatigue tests. However, to accurately evaluate the fatigue limit, a large number of fatigue specimens and test cycles are required, and the process is costly and time-consuming.

In general, the fatigue properties of materials are strongly correlated with tensile strength and hardness [1]. Especially in the context of steel materials, it is empirically known that there is a strong correlation between fatigue limit and tensile strength or hardness [2–4]. Murakami et al. [5] considered the effects of micro-surface defects, micro-surface crack shape and size, and Vickers hardness on the rotating bending and tensile-compressive fatigue limit and proposed an estimation formula by the square root $\sqrt{area}$ of the projected area of the surface defect in the direction of maximum principal stress. Furthermore, it is known that fatigue limits are related to grain size in low-strength steels [1,6]. These studies on estimating fatigue limits were primarily conducted utilizing the ordinary fatigue test procedure, with servo-hydraulic or electric motors serving as the driving force, up to a loading frequency of approximately 100 Hz.

Since the late 1990s, the fatigue fracture of metallic materials in the long-life region where the number of stress cycles exceeds 10^7 times has been reported, and the ultra-high cycle fatigue properties of metallic materials have attracted attention [7]. However, it takes a long time to conduct fatigue tests up to the ultra-high cycle region at normal loading frequency. From the viewpoint of reducing the test time, ultrasonic fatigue tests using ultrasonic technology have been conducted, and many studies have been conducted in recent years [8–16]. Nevertheless, it has been pointed out that the fatigue properties of some metallic materials are affected by the loading frequency [9,14]. In the 2000s, Papakyriacou et al. [11] reported that the fatigue limit of body-centered cubic pure tantalum in ultrasonic fatigue tests was much higher than that in conventional servo-hydraulic tests. Guennec et al. [10,17], Bech [16], and Torabian et al. [18] conducted fatigue tests at various loading rates to clarify the effect of the loading rate on the fatigue properties. As a result, it was found that the fatigue properties of low-carbon steel are significantly affected by the loading frequency.

Against this backdrop, Bennet [19] investigated the relationship between fatigue limit and loading frequency from a reaction kinetics perspective. They proposed an analytical model based on the strain dependence of yield strength, which can accurately explain the trend of experimental results with different loading frequencies. Toyosada et al. [20] proposed a constitutive equation for mild steel that accounts for the effects of strain rate and temperature. Tagawa et al. [21] developed a theoretical interpretation of the relation between the strain rate and yield strength in low-to-medium-strength steels. Guennec et al. [22] proposed a physical model of the loading frequency dependence of the fatigue limit of low-carbon steel based on the dislocation motion under cyclic loading. They reported that the fatigue limit of low- and medium-carbon steels, dependent on loading frequency, can be estimated by grouping data by axial-loading fatigue levels based on carbon content. In this study, rotating bending fatigue tests were conducted on low- and medium-carbon steels, and the estimation of the rotating bending fatigue limit in terms of the rate process theory proposed by Guennec et al. was attempted using a model [23]. As described above, the loading-frequency dependence of the fatigue limit of carbon steels with ferrite microstructures has been studied mainly for the axial-loading fatigue limit, which can be tested up to a high-frequency band. However, no studies have been conducted on the estimation of the loading-frequency-dependent fatigue limit of the rotating bending fatigue limit, which can be tested in a frequency band of about 100 Hz.

This study presents a strategy to extend the scope of the aforementioned model's application not only to axial-loading fatigue but also to rotating bending fatigue. Therefore, this paper is organized into five main sections. Section 1 describes the issues with the current methods of fatigue limit estimation that form the background of this study and the need for methods of fatigue limit estimation that consider the effect of loading frequency. Section 2 describes the method of performing rotating bending fatigue tests on low- and medium-carbon steels for machine structural purposes. Section 3 presents the results of rotating bending fatigue tests on low- and medium-carbon steels for machine-structural purposes. Section 4 compares the results of the rotating bending fatigue tests, which were conducted using the axial-loading model, in terms of the rate process theory presented by Guennec et al. in order to analyze the effect of the frequency component of the fatigue test results. Section 5 details the model extension procedure and contains an evaluation of the model's effectiveness.

2. Rotating Bending Fatigue Test

2.1. Materials

The specimens were rolled round bars of JIS S10C, JIS S25C, JIS S35C, and JIS S45C, and their chemical compositions are shown in Table 1. JIS S10C and JIS S25C were annealed at 600 °C for one hour, while JIS S35C and JIS S45C were used as received.

The hardness of each specimen was measured from the surface of the specimen in the depth direction using a Vickers hardness tester. Hardness measurements were obtained in 100 μm increments in the central direction from a position 100 μm from the top surface of the specimen's cross section. As the hardness distribution of the specimens was not uniform, the Vickers hardness was determined as the average of five points from the specimen surface to 500 µm. As a result, Vickers hardness values of 115 HV, 150 HV, 177 HV, and 247 HV were determined for JIS S10C, JIS S25C, JIS S35C, and JIS S45C, respectively.

Table 1. Chemical composition of each specimen (mass%).

	C	Si	Mn	P	S	Ni	Cu	Cr
JIS S10C	0.10	0.23	0.40	0.018	0.008	0.02	0.01	0.02
JIS S25C	0.25	0.19	0.41	0.021	0.019	0.06	0.10	0.12
JIS S35C	0.35	0.26	0.67	0.016	0.007	0.04	0.05	0.10
JIS S45C	0.45	0.20	0.72	0.015	0.014	0.01	0.01	0.16

2.2. Specimens

The shape and dimensions of a rotating bending fatigue test specimen are shown in Figure 1. A commercial round bar 13 mm in diameter was used and turned into an hourglass shape with a grip diameter of 10 mm, a tip diameter of 4 mm, and a radius of curvature of 10 mm. The surface was then polished with #800, #1200, and #2000 emery paper to remove the turning marks on the tip surface and buffed with 3 µm abrasive alumina to finish the surface. The elastic stress concentration factor in rotating bending fatigue is $K_t = 1.055$.

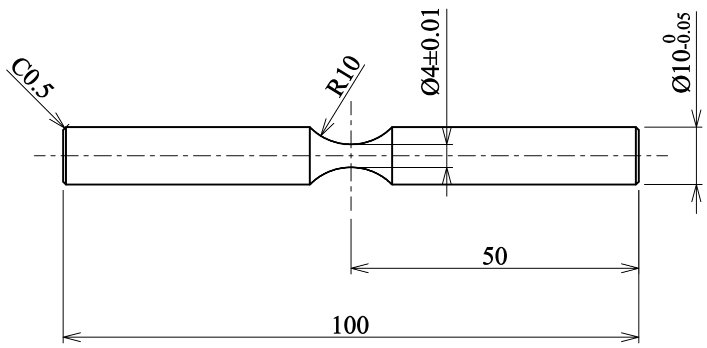

Figure 1. Configuration of the fatigue specimen.

2.3. Fatigue Testing Conditions

Rotating bending tests were performed using a dual-spindle rotating bending fatigue testing machine [24]. The fatigue testing machine consisted of an induction motor that transmitted power via a flat belt and rotated two spindles. Specimens were mounted on both ends of each spindle, and a dead-weight load was applied to them via a bearing situated at the tip. The maximum principal stress, σ, was set by a dead weight, W. The following equation was used to set a dead weight, W.

$$W = \frac{\sigma \pi d^3}{32 g K_t l} \tag{1}$$

where d is the tip diameter of the specimen, g is the acceleration of gravity, K_t is the elastic stress concentration factor, and l is the distance from the center of the specimen to the weight-loaded area. A photo sensor continuously detected the spindle rotations while the repetitions were counted. Once the specimen fractured, the device triggered a microswitch that halted the timer and presented the specimen's fracture life.

This fatigue testing machine can change the loading frequency by using an inverter in the induction motor driving unit. The minimum and maximum frequencies within the testable frequency range were tested. In this fatigue test, the loading frequency was set to 7 Hz and 70 Hz, and the fatigue tests were conducted as shown in Table 2. The fatigue tests were performed until failure or up to a limiting lifetime of 2×10^7 load cycles. The tests were performed in the air at room temperature.

Table 2. List of the loading frequencies for each specimen.

	Loading Frequency f, Hz	
	7	**70**
JIS S10C	-	Conduct
JIS S25C	-	Conduct
JIS S35C	Conduct	Conduct
JIS S45C	Conduct	Conduct

3. Fatigue Test Results

Figure 2a–d show the *S-N* diagrams obtained from the rotating bending fatigue tests involving JIS S10C, JIS S25C, JIS S35C, and JIS S45C, respectively, wherein the bilinear curves, represented by solid lines, were determined via a standard JSMS regression method [25]. The vertical axis, σ_a, is the stress amplitude, and the horizontal axis, N_f, is the number of cycles to failure. Figure 2 shows that the fatigue limit increases with increasing carbon content. The calculated fatigue limits are shown in Table 3. According to results reported in [26], the rotating bending fatigue limits of JIS S10C when annealed in a furnace at about 900 °C, and the limits of JIS S25C when annealed in a furnace at about 850 °C, are 135 to 245 MPa and 185 to 295 MPa, respectively. These fatigue test results are within a reasonable range. However, as reported in [26], the rotating bending fatigue limits of JIS S35C when annealed in a furnace at about 830 °C, as well as JIS S45C when annealed in a furnace at about 810 °C, are 195 to 295 MPa and 205 to 305 MPa, respectively. Although the heat treatment temperatures for JIS S10C and JIS S25C were different from those in the literature, the results were equivalent to the values described in the literature because the specimens were annealed. However, for JIS S35C and JIS S45C, hot-rolled bars were used as supplied. In general, annealing removes residual stresses and the hardening generated in the material during the material working process, resulting in lower fatigue limit values. The fatigue limit of JIS S45C is higher than that of materials with similar carbon content. This is considered to be due to the increase in static strength resulting from the presence of 0.5% or more of solid solution Mn [27,28].

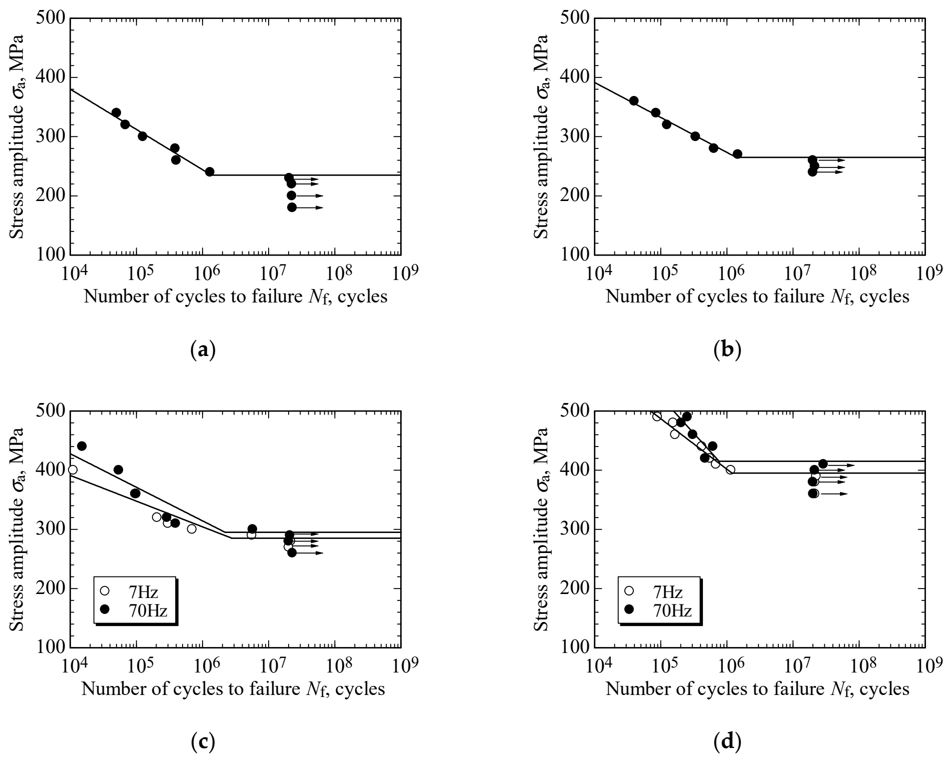

Figure 2. *S-N* diagram of each material: (**a**) JIS S10C, (**b**) JIS S25C, (**c**) JIS S35C, and (**d**) JIS S45C.

Table 3. List of rotating bending fatigue limits for each specimen.

	Loading Frequency f, Hz	Fatigue Limit σ_w, MPa
JIS S10C	70	235
JIS S25C	70	265
JIS S35C	7	285
	70	295
JIS S45C	7	395
	70	415

When comparing the fatigue test results of medium-carbon steel at 7 Hz and 70 Hz, the results for both JIS S35C and JIS S45C showed an increase in the fatigue limit of about 3–5%. In a study by Nishihara et al. [29], four low- and medium-carbon steels were tested in a rotating bending fatigue test at different loading frequencies ranging from 50 rpm (0.8 Hz) to 15,000 rpm (250 Hz), and the fatigue limit was reported to increase by about 7% at 0.4%C. Our fatigue test results are consistent with the results obtained by Nishihara et al. [29]. However, the fatigue limit is deemed to fall within the *S-N* curve's variation range, and it cannot be said that the fatigue limit's dependence on loading frequency has been observed.

For carbon steel, a model for estimating the fatigue limit in rotating bending based on hardness in the range of Vickers hardness H_v below 400 HV was proposed by Garwood [3]:

$$\sigma_w = 1.6H_v \pm 0.1H_v \tag{2}$$

where the unit for the fatigue limit σ_w is MPa. Figure 3 shows a comparison between Equation (2) and the fatigue test results. From the figure, the fatigue limit of each material was plotted to be higher than the estimated line of sight. It was confirmed that the fatigue test results were the same as those obtained using the conventional estimation method.

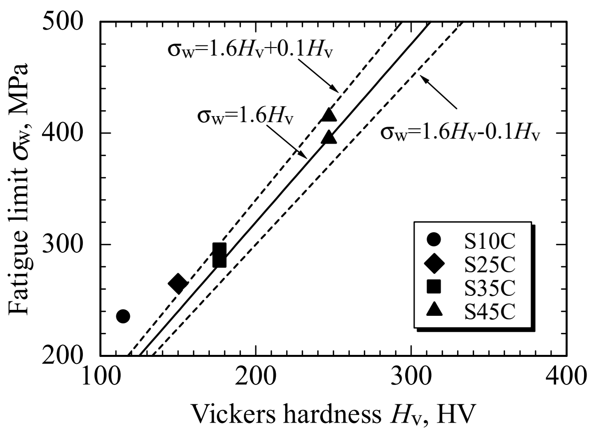

Figure 3. Results of estimating fatigue limit by using Vickers hardness.

4. Comparison of Fatigue Limits with Proposed Model Estimation

Guennec et al. [22,23] proposed an estimation equation based on the rate process theory for the thermal activation of dislocations because ferritic/pearlitic steels are BCC lattice materials, and the strain-rate dependence is high. The proposed equations are shown in Equations (3) and (4).

$$E = \alpha_0 \exp\left(\frac{\beta_0}{T_0 \ln\left(\frac{f_0}{f}\right)}\right) \tag{3}$$

$$f_0 = \frac{\dot{\varepsilon}_0}{2\Delta\varepsilon_E} \tag{4}$$

where α_0 and β_0 are the material parameters for when the temperature T_0 is 293 K, and f_0 is the frequency coefficient linking to the frequency corresponding to $\dot{\varepsilon}_0$, while $\Delta\varepsilon_E$ is the total strain range imposed by the fatigue test at the fatigue limit *E*. As, in the case of this study, the materials used were low- and medium-carbon steels with ferrite/pearlite microstructures, we assumed that $\Delta\varepsilon_E$ at the fatigue limit *E* was the same as that used by Guennec et al. [22,23], which was $\Delta\varepsilon_E = 0.002$. The frequency coefficient $\dot{\varepsilon}_0$ was assumed to be $\dot{\varepsilon}_0 = 10^7\ \mathrm{s}^{-1}$ based on the work of Conrad et al. [30] involving pure iron. By substituting these values into Equation (4), $f_0 = 2.5 \times 10^9 \mathrm{s}^{-1}$ was calculated and applied to Equation (3).

Guennec et al. [16] analyzed the relationship between the fatigue limit and the loading frequency for low- and medium-carbon steels with ferrite/pearlite microstructures by grouping them according to carbon content and analyzing material parameters α_0 and β_0 using the Pareto solution. As a result, the axial-loading model, in which the rate process theory is considered, was proposed, and the effect of loading frequency on the fatigue limit was different for each carbon content [23]. Figure 4 shows a plot of the rotating bending fatigue test results on the analytical model [23]. The solid line in the figure shows the model proposed by Guennec et al. The model is divided into three groups for each carbon content. When the rotating bending fatigue test results were classified to correspond to this model grouping, JIS S10C was compared with the model for the group with carbon contents between 0.08 and 0.11% (G1 Group), and JIS S35C and JIS S45C were compared with the model for the group with carbon contents between 0.33 and 0.46% (G3 Group). Although JIS S25C has no corresponding group in the proposed model, it was compared with models in the group with carbon contents between 0.12 and 0.22% due to its carbon content range being similar to that of the 0.12–0.22% group (G2 Group).

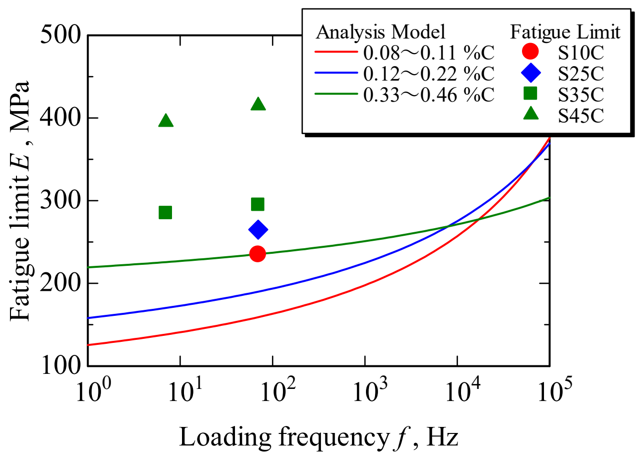

Figure 4. Comparison of the estimated fatigue limits derived from the proposed model and the actual rotating bending fatigue test results.

The estimated fatigue limits were calculated for the two loading frequencies of 7 Hz and 70 Hz used in this fatigue test and compared with the results of rotating bending fatigue tests at the corresponding loading frequencies. Table 4 shows the comparison results. The relative error between the estimated fatigue limit *E* obtained using the model and the rotating bending fatigue limit σ_w obtained through the rotating bending fatigue test was calculated using the formula $(\sigma_\mathrm{w} - E)/E$. As shown in the table, the relative error was more than +20% for all the data. In particular, JIS S35C and JIS S45C, which belong to the same group, showed a wide range of relative error from 25.3 to 76.3%. This difference can be attributed to differences in the magnitude of static strength, such as the hardness within each group. This result suggests that the static strength parameter should be considered in the model in terms of rate process theory.

Table 4. Results comparing estimated fatigue limits and fatigue test results.

Group	%C	Loading Frequency f, Hz	Estimated Fatigue Limit, MPa	Material	Fatigue Limit σ_w, MPa	Error, %
G1	0.08–0.01	70	159	JIS S10C	235	47.7
G2	0.12–0.22	70	190	JIS S25C	265	39.5
G3	0.33–0.46	7	226	JIS S35C	285	26.3
				JIS S45C	395	75.0
		70	235	JIS S35C	295	25.3
				JIS S45C	415	76.3

5. Discussion

5.1. Flow of Model Consideration

Factors that influence the fatigue behavior of metallic materials include the strain rate, microstructure, temperature, and strength. Therefore, we focus on material hardness, a factor whose influence is not considered in the axial-loading model in terms of rate process theory [23]. Material hardness is the ability of a material to resist loads from plastic deformation, and the strength values are determined by the chemical composition and structural properties. Cyclic softening and hardening are considered to be coupling factors that change the original strength state of the material and influence the tendency for loading frequency to have effects [13]. Therefore, material hardness was investigated as the primary factor. In this chapter, the flowchart shown in Figure 5 is used to validate and derive the equations.

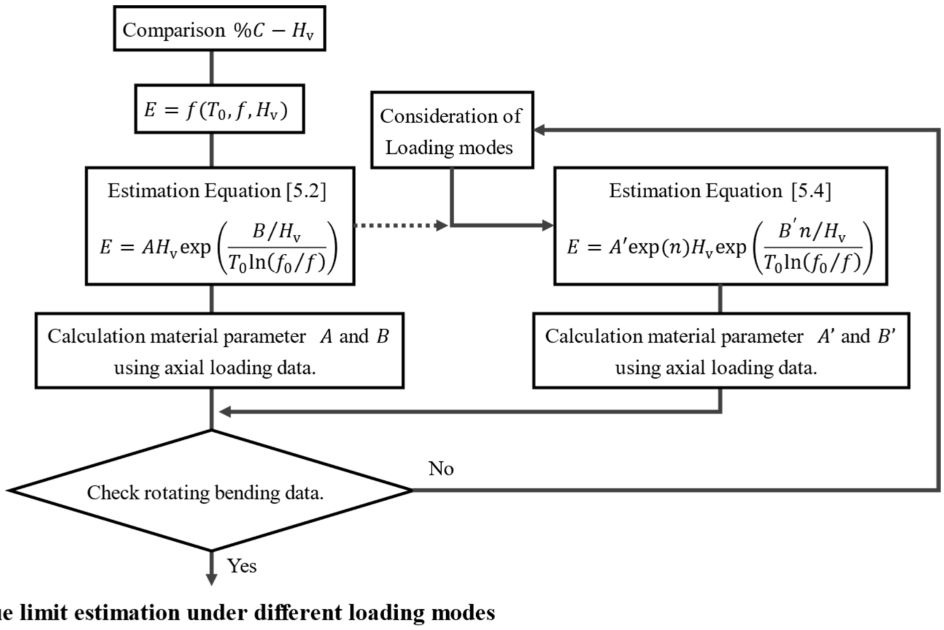

Figure 5. Flowchart of model derivation in this study.

First, the relationship between the hardness, loading frequency, and fatigue limit was investigated, and a model using the hardness parameter was proposed based on the data for the axial-loading fatigue limit. Next, we checked whether the proposed model was applicable to the rotating bending fatigue, which is a different loading mode from axial-loading fatigue. Finally, the effects of different loading modes on the parameters were clarified, and a new model for estimating the loading-frequency-dependent fatigue limits for different loading modes was proposed.

5.2. Studying Model Using Vickers Hardness

The confirmed relationship between carbon content and Vickers hardness in the data from Guennec et al. [23] was used to investigate factors that influence fatigue limit other than loading frequency. Figure 6 shows the results. Since Vickers hardness is not commonly defined in the literature, the following empirical equation was used to evaluate the relationship between tensile strength σ_B [MPa] and Vickers hardness.

$$\sigma_B \cong \frac{1}{3}(9.8 \times H_v) \cong 3.27 \times H_v \tag{5}$$

Figure 6 shows that Vickers hardness increases with increasing carbon content, indicating a positive correlation between the two. The least-square method was used for linear regression, with each plotted point shown by the solid line. The Fe-C phase diagram demonstrates that carbon steels with ferrite/pearlite microstructures experience an increase in pearlite volume fraction as ferrite volume fraction decreases. Hirukawa et al. [31] established a proportional relationship between tensile strength and pearlite volume fraction by decomposing tensile strength into strengthening mechanisms based on the Hall–Petch rule and relating them to microstructural parameters. The Fe-C phase diagram shows that the volume fraction of pearlite increases as the volume fraction of ferrite decreases in carbon steels with ferrite/pearlite microstructures. The trend shown in Figure 6 is due to the increase in the volume fraction of pearlite.

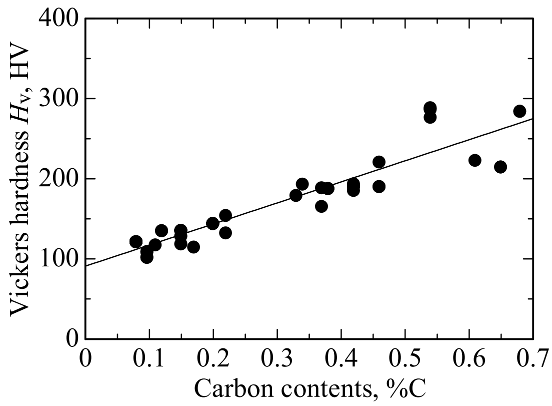

Figure 6. Relationship between carbon contents and Vickers hardness.

Below, Figure 7 shows the relationship between the axial-loading fatigue limit and the Vickers hardness. The dotted line in the figure is an empirical relationship equation between the Vickers hardness H_v and the axial-load fatigue limit σ_w in a double-ended tension-compression fatigue test for steel materials with a Vickers hardness H_v of 400 HV or less, as shown in Equation (6) [4].

$$\sigma_w = 1.47 H_v \tag{6}$$

The fatigue limit data utilized in this study were derived from the work of Guennec et al. [16]. Based on Figure 7, when the loading frequency is less than 100 Hz, the relationship between the fatigue limit and Vickers hardness can be described by Equation (6). However, at frequencies exceeding 100 Hz, the correlation between the axial-load fatigue limit and Vickers hardness diverges from the conditions of Equation (6). This finding is significant for materials with Vickers hardness values below 150 HV.

Therefore, a three-dimensional plot was made to evaluate the relationship between Vickers hardness, loading frequency, and fatigue limit. The results are shown in Figure 8. All plot points were regressed using a quadratic shape regression surface. The correlation coefficient, r, displays a strong correlation at 0.944. Figures 7 and 8 show that Vickers hardness and loading frequency are both factors that affect the fatigue limit.

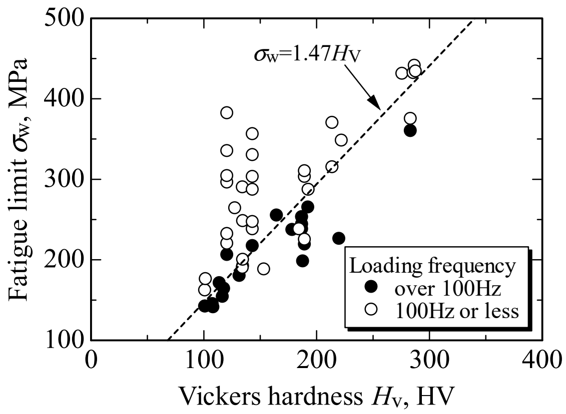

Figure 7. The axial-loading relationship between fatigue limit and Vickers hardness.

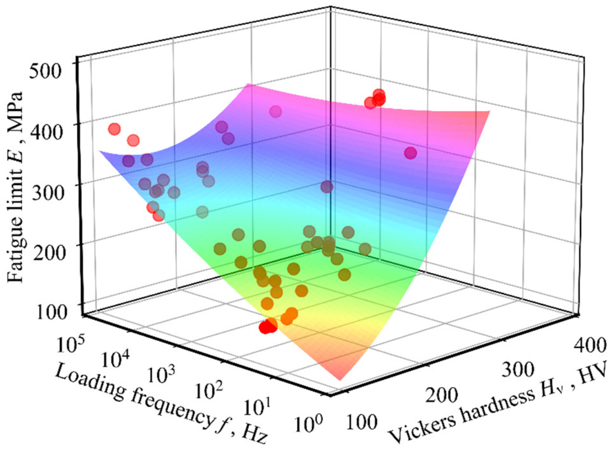

Figure 8. Overview of the selected fatigue limit data [16], expressed alongside data for the Vickers hardness and loading frequency. Second-order surface fitting is included for illustrative purposes.

Based on Equation (3), the smaller the value of the material parameter β_0, the smaller the effect of the loading frequency on the fatigue limit. The effect of the loading frequency on the fatigue limit tends to decrease as the Vickers hardness value increases, as shown in Figure 8. Based on the above, we proposed Equation (7) by reflecting these contents in the material parameters α_0 and β_0 in Equation (3).

$$E = AH_{\mathrm{v}}\exp\left(\frac{B/H_{\mathrm{v}}}{T_0\ln\left(\frac{f_0}{f}\right)}\right) \tag{7}$$

where A and B are material parameters. A and B were estimated from axial-loading fatigue data [23]. E/H_{V} was used for the vertical axis, and $\exp((1/H_{\mathrm{V}})/T_0\ln(f_0/f))$ was used for the horizonal axis. Each axis was converted to a logarithmic axis and subjected to linear regression using the least-square method. The intercept and slope obtained through linear regression were utilized as the material parameters A and B, which are shown in Equation (8):

$$E = 0.908H_{\mathrm{v}}\exp\left(\frac{3.68\times10^5/H_{\mathrm{v}}}{T_0\ln\left(\frac{f_0}{f}\right)}\right) \tag{8}$$

The correlation coefficient, r, displays a strong correlation at 0.8. The model outcomes are presented via the three-dimensional diagram shown in Figure 9a.

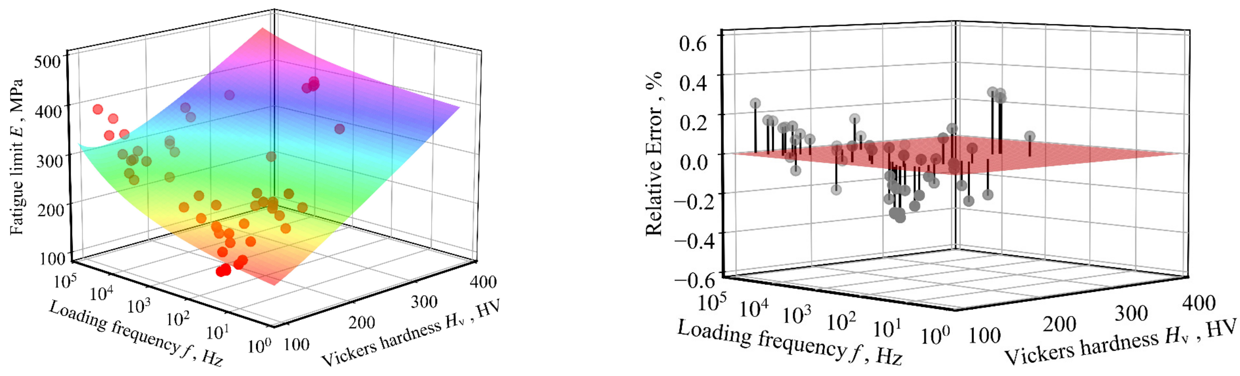

(**a**) (**b**)

Figure 9. (**a**) A three-dimensional plot showing the results derived from the extended model; (**b**) a representation of the relative error for the selected axial-loading fatigue limit data [16].

For each axial-loading fatigue datum, the relative error of the fatigue limit estimation, provided by the $(\sigma_\mathrm{w} - E)/E$ calculation, was subsequently plotted, as shown in Figure 9b. The percentages of data within ±10% and ±20% of the relative error were 44% and 80%, respectively. From the above, we have concluded that it is valid to express material parameters in terms of Vickers hardness.

5.3. Examining the Effects of Different Loading Modes

We examined the differences in values between the axial-loading model established in terms of the rate process theory [23] put forth by Guennec et al. in Section 4 and the rotating bending fatigue test results, using various data on the rotating bending fatigue limit, to see whether the difference was "due to the effect of the difference in static strength" or "due to the effect of the difference in loading mode". The axial-loading model established in terms of the rate process theory [23] was proposed based on the results of fatigue tests under axial loading fatigue with a stress ratio of $R = -1$ on carbon steel with a duplex ferritic/pearlitic microstructure that has not undergone hardening and tempering. Since the number of data is insufficient for comparison with the fatigue test results in this study, the literature values were used for comparison with the data under axial-loading fatigue [23]. In comparing the axial-loading fatigue limit, the literature values were examined based on the following four conditions, except for the discrepancy caused by the loading mode. However, the loading frequency was limited to 120 Hz because the mechanism by which the rotating bending fatigue test is conducted does not allow fatigue tests in the high-frequency band as in the axial-loading fatigue test.

1. The microstructure of the carbon steel was predominantly duplex ferritic/pearlitic, except for strongly quenched steels. Moreover, cases involving ultrafine grain structures are outside the scope of the proposed model.
2. Fatigue tests were operated in air and at room temperature under rotating bending. The test environment in which the specimens were subjected to high temperatures was excluded.
3. The specimen shape inferred a stress concentration factor K_t less than 1.15.
4. The loading frequency of the fatigue test was within a wide range spanning from 1 to 120 Hz.

In accordance with these criteria, a total of 23 fatigue limit data were collected. Details on the selected data are shown in Table 5 [32–38].

Table 5. General information on the selected fatigue data.

Data No.	%C	H_V	*f*, Hz	σ_W,Mpa	Ref.
1	0.09	115	57	162	[32]
2	0.1	115	70	235	This study
3	0.1	103	18.3	186	[33]
4	0.11	155	57	235	[32]
5	0.12	142	28.3	177	[34]
6	0.13	119	50	205	[35]
7	0.21	135	60	200	[36]
8	0.21	141	50	235	[37]
9	0.25	149	70	265	This study
10	0.27	153	50	273	[38]
11	0.28	143	50	258	[38]
12	0.35	177	7	285	This study
13	0.35	177	70	295	This study
14	0.44	174	50	245	[37]
15	0.45	225	7	395	This study
16	0.45	225	70	415	This study
17	0.46	192	50	308	[38]
16	0.46	261	50	436	[38]
19	0.47	196	50	320	[38]
20	0.47	270	50	421	[38]
21	0.49	199	50	328	[38]
22	0.49	266	50	452	[38]
23	0.54	177	50	255	[38]

The relationship between the axial-loading fatigue limit and the rotating bending fatigue limit was checked using three-dimensional plots. The results are shown in Figure 10. All plot points (the axial-loading fatigue limit and the rotating bending fatigue limit) were regressed using a quadratic shape regression surface. The correlation coefficient, *r*, displays a strong correlation at 0.922. It can be expressed by one common surface despite the different loading modes.

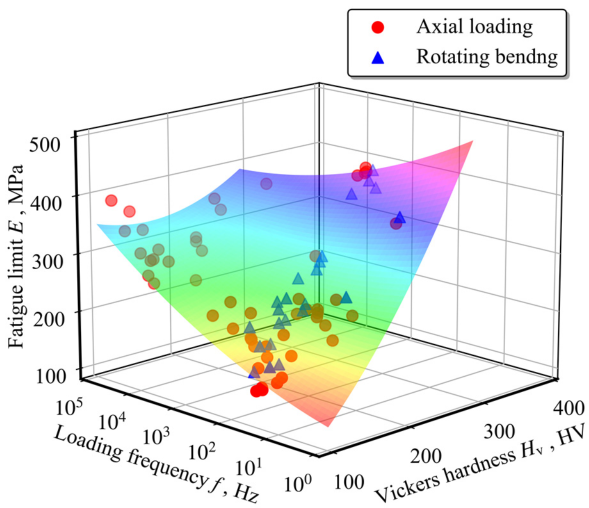

Figure 10. Overview of the selected fatigue limit data, expressed alongside the Vickers hardness and loading frequency, including two different types: axial loading [16] and rotating bending. Second-order surface fitting is included for illustrative purposes.

The relationship between the model and the rotating bending fatigue limit when using Equation (8) is shown in Figure 11a. For each selected rotating bending fatigue datum, the relative error of the fatigue limit estimation, provided by the $(\sigma_W - E)/E$ calculation, was then plotted in Figure 11b. The percentages of data within ±10% and ±20% of the relative error were 26% and 48%, respectively. In several datasets, the rotating bending fatigue limit was greater than that of the model based on Equation (8). This is similar to the tendency of the equation for estimating the fatigue limit from Vickers hardness, which is empirically known by Equations (2) and (6), for different loading modes. This suggests that differences in loading modes need to be considered when estimating fatigue limits using the proposed model.

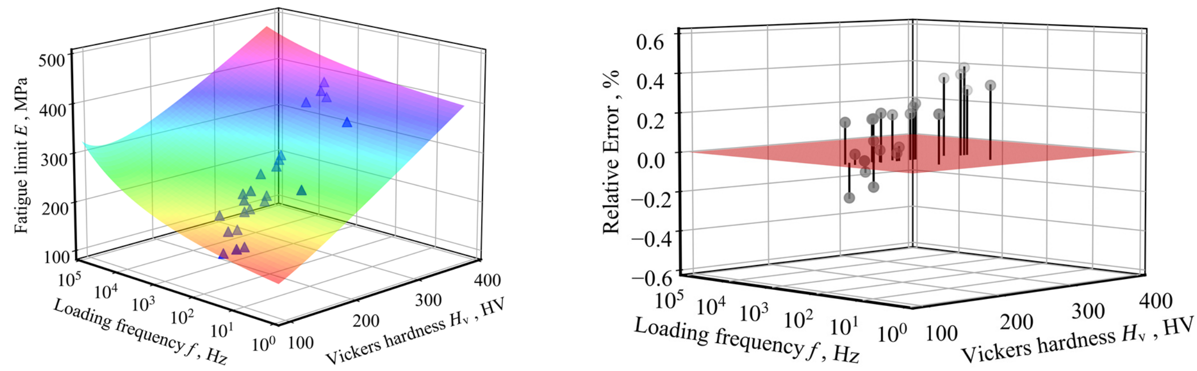

(**a**) (**b**)

Figure 11. (**a**) A three-dimensional plot of the results derived from the extended model; (**b**) a representation of the relative error for every selected datum.

5.4. Proposing the Model in Terms of the Rate Process Theory

In terms of rate process theory proposed by Guennec et al. [22,23], the estimation equation on which our model was based is based on an Arrhenius-type equation. The material parameters α_0 and β_0 in the estimation equation in terms of the rate process theory shown in Equation (3) are considered to contain information on the mode of loading. Equation (9), which shows the stress dependence of the strain rate during steady-state creep deformation, is also an Arrhenius-type equation [39].

$$\dot{\varepsilon} = \dot{\varepsilon_0}\left(\frac{\sigma}{G}\right)^n \exp\left(-\frac{U_a}{RT}\right) \tag{9}$$

where n is the stress index, σ is the loading stress, G is the shear modulus, U_a is the activation energy, R is the gas constant, and T is the absolute temperature. Equation (9) was transformed logarithmically into the relationship between applied stress and strain rate shown in Equation (10):

$$\sigma = G\exp(n)\exp\left(nU_a/\left(RT\ln\left(\dot{\varepsilon}/\dot{\varepsilon_0}\right)\right)\right) + G\left(\dot{\varepsilon}/\dot{\varepsilon_0}\right) \tag{10}$$

Equation (10) shows that the strain rate at applied stress varies with the stress index n. Similar to the rate process theory [22,23], Equation (10) relates the loading frequency at the fatigue limit stress, E, at a room temperature of 293K. By substituting Equation (4) into Equation (10), we obtained Equation (11):

$$E = G\exp(n)\exp(nU_a/(RT\ln(f/f_0))) + G(f/f_0) \tag{11}$$

Comparing Equations (7) and (11), focusing on the relationship between loading frequency and stress, the material parameters A and B in Equation (7) can be expressed as $A = \exp(n)\ A'$ and $B = nB'$. Substituting these relationships into Equation (7), we obtain Equation (12):

$$E = A'\exp(n)H_v\exp\left(\frac{B'\frac{n}{H_v}}{T_0\ln\left(\frac{f_0}{f}\right)}\right) \tag{12}$$

where A' and B' are the material parameters. The stress index n varies depending on the activation volume [40]. Since the activation volume is known to be subject to change in axial-loading fatigue tests and rotating bending fatigue tests, the stress index was applied to the model as a difference in loading mode.

Here, axial-loading fatigue, which can be tested up to a high-frequency band, is considered as a standard. We calculated the material parameters A' and B' in Equation (11) by assuming that the stress index in the axial-loading fatigue was $n = 1$. The material parameters A' and B' were estimated from axial-loading fatigue data [9]. $E/(\exp(n)H_V)$ was used for the vertical axis, and $\exp((n/H_V)/T_0\ln(f_0/f))$ was used for the horizonal axis. Each axis was converted to a logarithmic axis and subjected to linear regression using the least-square method. The intercept and slope obtained through linear regression were utilized as the material parameters A' and B', which are shown in Equation (13):

$$E = 0.334\exp(n)H_v\exp\left(\frac{3.68\times10^5\times\frac{n}{H_v}}{T_0\ln\left(\frac{f_0}{f}\right)}\right) \tag{13}$$

Based on the fatigue limit estimation equations using the Vickers hardness shown in Equations (2) and (6), the coefficients used in the estimation depend on the loading mode, even for the same Vickers hardness. In cases of double-swing tensile and compressive fatigue, such as axial-loading fatigue, the coefficient value of the loading mode is 1.47 for Vickers hardness, and in the case of rotating bending fatigue, the coefficient value of the loading mode is 1.6 for Vickers hardness. If the reference value is double-sided tensile and compressive fatigue, such as axial-loading fatigue, the coefficient ratio between the rotating bending fatigue and axial-loading fatigue is $1.6/1.47 \cong 1.09$. This coefficient ratio was calculated based on the loading mode, and it indicates that the difference is dependent on the loading mode. Therefore, this difference was considered as a value that represents the effect of loading style on the stress index.

Figure 12a compares the model with the stress index in rotating bending fatigue with a three-dimensional plot of the rotary interlock fatigue limit. The following equation was used for the model, along with a stress exponent n of $n = 1.6/1.47 \cong 1.09$ for Equation (14), which is as follows:

$$E = 0.334\exp(1.09)H_v\exp\left(\frac{3.68\times10^5\times\frac{1.09}{H_v}}{T_0\ln\left(\frac{f_0}{f}\right)}\right) \tag{14}$$

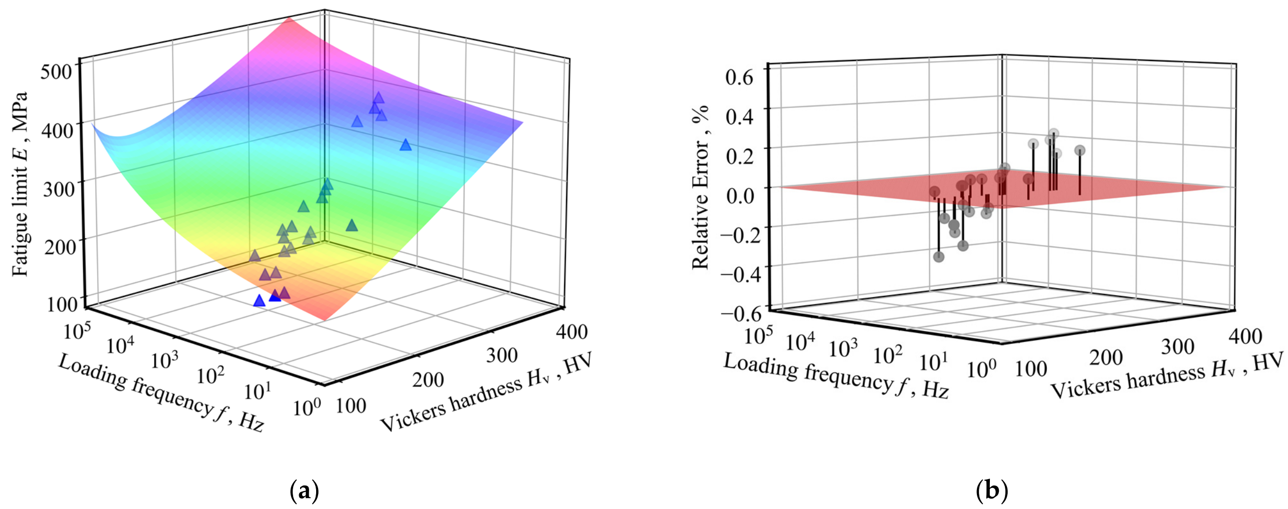

Figure 12. (**a**) A three-dimensional plot showing results derived from the extended model; (**b**) a representation of the relative error for every selected rotating bending fatigue datum.

The relative error of the fatigue limit estimation, provided by the $(\sigma_w - E)/E$ calculation, was subsequently plotted, as shown in Figure 11b. The percentages of data within $\pm 10\%$ and $\pm 20\%$ of relative error were 50% and 73%, respectively. Compared to the estimation results obtained without considering the loading mode, these results were judged to be the result of improved accuracy due to the use of the stress index.

Ishii et al. [41] showed that, in their study, the ratio of rotating bending fatigue to axial-loading fatigue was almost identical, assuming the effect of the restraint to be 0.9, because, in the case of rotating bending fatigue, the plastic deformation that occurs only on the surface is restrained by the internal elastic deformation, and the actual acting stress is higher than the evaluated stress. The ratio of axial-loading fatigue to rotating bending fatigue is $1/0.9 \cong 1.11$, which is close to the ratio of 1.09 estimated by the equation using Vickers hardness H_v for axial-loading fatigue and rotating bending fatigue. It is thought that the effect of the loading frequency on the fatigue limit of the rotating bending fatigue is larger than that of the axial loading fatigue because of the plastic deformation of the surface of the material.

Based on the above, by using the stress index as a loading-mode coefficient, it is possible to estimate the loading frequency-dependent rotating bending fatigue test limit based on the results of axial-loading fatigue tests, which can be conducted up to high-frequency bands.

6. Conclusions

This study presents a new formula for estimating the rotating bending fatigue limit in terms of Vickers hardness and loading frequency as parameters for low-carbon and medium-carbon steels. In other words, it became possible to estimate the rotating bending fatigue limit by transforming the formula for fatigue limit estimation under axial-loading fatigue that was proposed by Guennec, based on the rate process theory, into a formula that added material hardness and stress index. The loading frequency and hardness of carbon steel were found to be important parameters in explaining the fatigue limit of the material. The main conclusions from this study can be summarized as follows:

1. The fatigue limits were compared with the axial-loading model in terms of the rate process theory based on carbon content proposed by Guennec et al. and the results of the rotating bending fatigue test. A significant difference was observed, especially in the medium-carbon steel group. It was concluded that this result was caused by differences in static strength such as hardness within the same group.
2. Three-dimensional plots were used to confirm the relationship between loading frequency, Vickers hardness, and fatigue limit. The results revealed that loading frequency and Vickers hardness mutually influence the fatigue limit. That is, the effect of loading frequency on the fatigue limit was greater for materials with smaller Vickers hardness, and the effect of loading frequency on the fatigue limit was smaller for materials with larger Vickers hardness.
3. We considered the adoption of the stress index with reference to the basic equation of creep, which expresses the dependence of stress on the strain rate. We also proposed a new fatigue-estimation formula that expresses the loading-frequency dependence of the fatigue limit using the Vickers hardness and stress index.
4. The stress index in the newly proposed fatigue limit estimation formula was used as a parameter representing the influence of the type of load. It was suggested that the fatigue limit can be estimated by setting the stress index to $n = 1$ for axial-loading fatigue and $n = 1.09$ for rotating bending fatigue.

Author Contributions: Conceptualization, M.F. and N.O.; methodology, B.G.; investigation, M.F. and N.O.; project administration, N.H. and T.S. All authors have read and agreed to the published version of the manuscript.

Funding: This research received no external funding.

Institutional Review Board Statement: Not applicable.

Informed Consent Statement: Not applicable.

Data Availability Statement: The data presented in this study are available in the article.

Conflicts of Interest: The authors declare no conflict of interest.

References

1. Pang, J.C.; Li, S.X.; Wang, Z.G.; Zhang, Z.F. General relation between tensile strength and fatigue strength of metallic materials. *Mater. Sci. Eng. A* **2013**, *564*, 331–341. [CrossRef]
2. Pang, J.C.; Li, S.X.; Wang, Z.G.; Zhang, Z.F. Relations between fatigue strength and other mechanical properties of metallic materials. *Fatigue Fract. Eng. Mater. Struct.* **2014**, *37*, 958–976. [CrossRef]
3. Garwood, M.F. Correlation of Laboratory Tests and Service Performance, Interpretation of Tests and Correlation with Service. *ASM* **1951**, 1–77.
4. Nakamura, T. Fundamental Knowledge of Metal Fatigue. *J. Jpn. Foundry Eng. Soc.* **2007**, *79*, 58–69. [CrossRef]
5. Murakami, Y.; Kodama, S.; Shizuyo, K. Quantitative Evaluation of Effects of Nonmetallic Inclusions on Fatigue Strength of High Strength Steel. *Trans. Jpn. Soc. Mech. Eng. Ser. A* **1988**, *54*, 688–696. [CrossRef]
6. McGreevy, T.E.; Socie, D.F. Competing roles of microstructure and flaw size. *Fatigue Fract. Eng. Mater. Struct.* **1999**, *22*, 459–542. [CrossRef]
7. Stanzl-Tschegg, S.E. Fracture mechanisms and fracture mechanics at ultrasonic frequencies. *Fatigue Fract. Eng. Mater. Struct.* **1999**, *22*, 567–579. [CrossRef]
8. Kawamoto, M.; Tabuchi, S. Speed Effect in Fatigue Strength of Metals. *J. Jpn. Soc. Test. Mater.* **1960**, *9*, 452–458. [CrossRef]
9. Taira, S.; Emura, K. Investigation on the High Frequency Fatigue (The 1st Report). *J. Soc. Mater. Sci.* **1963**, *12*, 536–541. [CrossRef]
10. Guennec, B.; Ueno, A.; Sakai, T.; Takanashi, M.; Itabashi, Y. Effect of the loading frequency on fatigue properties of JIS S15C low carbon steel and some discussions based on micro-plasticity behavior. *Int. J. Fatigue* **2014**, *666*, 29–38. [CrossRef]
11. Papakyriacou, M.; Mayer, H.; Pypen, C.; Plenk, M., Jr.; Stanzl-Tschegg, S. Influence of loading frequency on high cycle fatigue properties of b.c.c. and h.c.p. metals. *Mater. Sci. Eng. A* **2001**, *308*, 143–152. [CrossRef]
12. Marti, N.; Favier, V.; Saintier, N.; Gregori, F. Investigating Fatigue Frequency Effects on Single Phase Ductile Materials. *Procedia Eng.* **2015**, *133*, 294–298. [CrossRef]
13. Nonaka, I.; Setowaki, S.; Ichikawa, Y. Effect of load frequency on high cycle fatigue strength of bullet train axle steel. *Int. J. Fatigue* **2014**, *60*, 43–47. [CrossRef]
14. Kikukawa, M.; Ohji, K.; Ogura, K. Push-Pull Fatigue Strength of Mild Steel at Very High Frequencies of Stress up to 100 kc/s. *ASME J. Basic Eng.* **1965**, *87*, 857–864. [CrossRef]
15. Tsutsumi, N.; Murakami, Y.; Doquet, V. Effect of test frequency on fatigue strength of low carbon steel. *Fatigue Fract. Eng. Mater. Struct.* **2009**, *32*, 473–483. [CrossRef]
16. Bach, J.; Möller, J.J.; Göken, M.; Bitzek, E.; Höppel, H.W. On the transition from plastic deformation to crack initiation in the high- and very high-cycle fatigue regimes in plain carbon steels. *Int. J. Fatigue* **2016**, *93*, 281–291. [CrossRef]
17. Guennec, B.; Ueno, A.; Sakai, T.; Takanashi, M.; Itabashi, Y.; Ota, M. Dislocation-based interpretation on the effect of the loading frequency on the fatigue properties of JIS S15C low carbon steel. *Int. J. Fatigue* **2015**, *70*, 328–341. [CrossRef]
18. Torabian, N.; Favier, V.; Dirrenberger, J.; Adamski, F.; Ziaei-Rad, S.; Ranc, N. Correlation of the high and very high cycle fatigue response of ferrite based steels with strain rate-temperature conditions. *Acta Mater.* **2017**, *134*, 40–52. [CrossRef]
19. Bennett, P.E. Parameter Representation of Low-Temperature Yield Behavior of Body-Centered Cubic Transition Metals. *J. Fluids Eng.* **1966**, *88*, 518–524. [CrossRef]
20. Toyosada, M.; Goto, K. Constitutive Equation for Mild Steel involved The Effect of Strain Rate and Temperature. *Trans. West-Jpn. Soc. Nav. Archit.* **1991**, *81*, 259–268.
21. Tagawa, T. Basic Mechanical Testing and Evaluated Material Properties. *J. Jpn. Weld. Soc.* **2008**, *77*, 40–47. [CrossRef]
22. Guennec, B.; Takahashi, J.; Oguma, N.; Sakai, T. Rate Process Analysis of the Loading Frequency Effect on the Fatigue Endurance of Low Carbon Steel. *J. Soc. Mater. Sci. Jpn.* **2019**, *68*, 235–241. [CrossRef]
23. Guennec, B.; Kinoshita, T.; Horikawa, N.; Oguma, N.; Sakai, T. Loading frequency effect on the fatigue endurance of structural carbon steels: Estimation based on dislocation motion theory and experimental verification of the model. *Int. J. Fatigue* **2023**, *172*, 107634. [CrossRef]
24. Sakai, T.; Takeda, M.; Shiozawa, K.; Ochi, Y.; Nakajima, M.; Nakajima, T.; Oguma, N. Experimental Reconfirmation of Characteristic S-N Property for High Carbon Chromium Bearing Steel in Wide Life Region in Rotating Bending. *J. Soc. Mater. Sci.* **2000**, *49*, 779–785. [CrossRef]
25. Sakai, T.; Sugeta, A. Publication of the Second Edition of "Standard Evaluation Method of Fatigue Reliability for Metallic Materials" [Standard Regression Method of S-N curves]. *J. Soc. Mater. Sci.* **2005**, *54*, 37–43. [CrossRef]
26. *Mechanical System Design Handbook Based on JIS*; Japanese Standards Association: Tokyo, Japan, 1986.
27. Yokobori, T.; Maekawa, I.; Korekawa, S. The Influence of Non-metallic Inclusions on the Fatigue Strength and the Statistical Nature of Steel. *J. Soc. Mater. Sci.* **1963**, *117*, 12. [CrossRef]

28. Shirawa, H.; Kobayashi, H.; Jizaimaru, J. The Effect of Various Strengthening Methods on Ductility of High Strength Steel Sheets. *Tetsu-to-Hagane* **1981**, *67*, 2208–2215. [CrossRef]
29. Nishihara, T.; Murase, O. The Effects of the repeating Speeds on the Fatigue of metallic Materials. *Trans. Jpn. Soc. Mech. Eng.* **1951**, *17*, 107–113. [CrossRef]
30. Conrad, H.; Frederick, S. The effect of temperature and strain rate on the flow stress of iron. *Acta Metall.* **1962**, *10*, 1013–1020. [CrossRef]
31. Hirukawa, H.; Matsuoka, S. Nanoscopic Strength Analysis of Ferrite-Pearlite Steels. *Trans. Jpn. Soc. Mech. Eng. Ser. A* **2002**, *68*, 1038–1045. [CrossRef]
32. Tokaiji, K.; Ando, Z.; Ushida, M.; Asahara, C. Effect of Overstressing on Fatigue Limit of Low Carbon Steel under Rotating Bending and Torsion. *J. Soc. Mater. Sci. Jpn.* **1976**, *25*, 863–869. [CrossRef]
33. NIishihara, T.; Taira, S.; Tanaka, K.; Koterazawa, R.; Azuma, Y. Fatigue of Low Carbon Steel at Elevated Temperature. *Trans. Jpn. Soc. Mech. Eng.* **1958**, *24*, 445–452. [CrossRef]
34. Ando, Z.; Kato, Y.; Watari, H. An Experiment on Fatigue of Low Carbon Steel at High Temperatures. *Trans. Jpn. Soc. Mech. Eng.* **1956**, *22*, 851–855. [CrossRef]
35. Kang, M.; Aono, Y.; Noguchi, H. Effect of Prestrain Type on the Rotating Bending Fatigue Limit of Carbon Steel. *J. Solid Mech. Mater. Eng.* **2008**, *2*, 82–94. [CrossRef]
36. Nisitani, H.; Fukuda, T. Fatigue Limit and Small-Crack Growth Law in Rotating Bending and Torsional Fatigue of Isotropic Carbon Steel Plain Specimens. *Trans. Jpn. Soc. Mech. Eng. Ser. A* **1993**, *59*, 311–318. [CrossRef]
37. Nisitani, H.; Fukuda, T. Relation between S-N Curve and Small-Crack Growth Law in Torsional Fatigue of Annealed Carbon Steel Plain Specimens. *Trans. Jpn. Soc. Mech. Eng. Ser. A* **1989**, *55*, 710–717. [CrossRef]
38. Nishijima, S. Scatter of Fatigue Strength in Medium Carbon Steels. *J. Soc. Mater. Sci.* **1974**, *23*, 9–14. [CrossRef]
39. Kikuchi, S.; Adachi, M. Deformation Behaviors of Metals and Alloys at Elevated Temperatures. *J. Soc. Mater. Sci. Jpn.* **1981**, *30*, 94–101. [CrossRef]
40. Nishino, K.; Honma, H. A Study on Temperature and Strain Rate Dependences of Yield Stress, and Ductile-Brittle Transition in Mild Steel. *Tetsu-to-Hagane* **1970**, *56*, 859–868. [CrossRef]
41. Ishii, A.; Nihei, M.; Kanazawa, K.; Nishijima, S. Prediction of Missing Properties in Fatigue Databases. *J. Soc. Mater. Sci. Jpn.* **1990**, *39*, 1285–1291. [CrossRef]